Atmos. Chem. Phys., 8, 1661–1675, 2008
www.atmos-chem-phys.net/8/1661/2008/


Atmospheric Chemistry and Physics

# Robust relations between CCN and the vertical evolution of cloud drop size distribution in deep convective clouds

**E. Freud**[1,2], **D. Rosenfeld**[1], **M. O. Andreae**[3], **A. A. Costa**[4], **and P. Artaxo**[5]

[1]Institute of Earth Sciences, The Hebrew University of Jerusalem, Jerusalem, Israel
[2]Department of Applied Environmental Sciences, Stockholm University, Stockholm, Sweden
[3]Biogeochemistry Department, Max Planck Institute for Chemistry, Mainz, Germany
[4]Department of Geology and Geophysics, Yale University, CT, USA
[5]Institute of Physics, Sao Paulo University, Brazil

Received: 24 June 2005 – Published in Atmos. Chem. Phys. Discuss.: 19 October 2005
Revised: 6 February 2008 – Accepted: 6 February 2008 – Published: 18 March 2008

**Abstract.** In-situ measurements in convective clouds (up to the freezing level) over the Amazon basin show that smoke from deforestation fires prevents clouds from precipitating until they acquire a vertical development of at least 4 km, compared to only 1–2 km in clean clouds. The average cloud depth required for the onset of warm rain increased by ∼350 m for each additional 100 cloud condensation nuclei per $cm^3$ at a super-saturation of 0.5% ($CCN_{0.5\%}$). In polluted clouds, the diameter of modal liquid water content grows much slower with cloud depth (at least by a factor of ∼2), due to the large number of droplets that compete for available water and to the suppressed coalescence processes. Contrary to what other studies have suggested, we did not observe this effect to reach saturation at 3000 or more accumulation mode particles per $cm^3$. The $CCN_{0.5\%}$ concentration was found to be a very good predictor for the cloud depth required for the onset of warm precipitation and other microphysical factors, leaving only a secondary role for the updraft velocities in determining the cloud drop size distributions.

The effective radius of the cloud droplets ($r_e$) was found to be a quite robust parameter for a given environment and cloud depth, showing only a small effect of partial droplet evaporation from the cloud's mixing with its drier environment. This supports one of the basic assumptions of satellite analysis of cloud microphysical processes: the ability to look at different cloud top heights in the same region and regard their $r_e$ as if they had been measured inside one well developed cloud. The dependence of $r_e$ on the adiabatic fraction decreased higher in the clouds, especially for cleaner conditions, and disappeared at $r_e \geq \sim 10\,\mu$m. We propose that droplet coalescence, which is at its peak when warm rain is formed in the cloud at $r_e = \sim 10\,\mu$m, continues to be significant during the cloud's mixing with the entrained air, cancelling out the decrease in $r_e$ due to evaporation.

*Correspondence to:* E. Freud
(eyal.freud@mail.huji.ac.il)

## 1 Introduction

During every dry season in Amazonia, many thousands of forest- and agricultural fires are set by the land owners and farmers, thus creating the "biomass burning" season. A deforestation rate of about 24 000 $km^2$ $year^{-1}$ causes the smoke emitted from the fires to cover vast areas. The smoke particles are quite efficient as cloud condensation nuclei (CCN), with 40–60% nucleation activity (CCN/CN ratio) at supersaturation (henceforth SS) of 1% (Andreae et al., 2004). Therefore the smoke and other small aerosols cause the formation of an increased number of small droplets for a given amount of cloud water, as Twomey (1974 and 1977) has suggested. This anthropogenic effect on clouds has already been documented using remote sensing methods (e.g., Coakley et al., 1987; Radke et al., 1989 (both showing ship tracks) and Kaufman and Fraser, 1997), in-situ measurements (e.g., Eagan et al., 1974; Costa et al., 2000 and Andreae et al., 2004) and cloud models (e.g., Khain et al., 2004). The smaller droplets will not coalesce efficiently to form precipitation particles. Rosenfeld (1999), Rosenfeld and Woodley (2003) and Rosenfeld et al. (2002) have shown, using satellite images and radar echoes, that polluted clouds have to develop to heights of more than 6 km in order to precipitate, compared to only 3 km in clean clouds. The change in vertical distribution of the precipitation processes causes changes in latent heat release (Andreae et al., 2004). In addition, the smoke

both absorbs and scatters sunlight, causing the ground to cool and the smoky layers to heat up, which stabilizes the lower troposphere and can inhibit the formation of new clouds (Koren et al., 2004). These two types of aerosol induced changes (cloud mediated and direct or semi-direct radiative forcings) can transfer the perturbations to much larger scales (Nober et al., 2003). The inadequate knowledge about these processes and the resulting great uncertainty are main reasons for climate models being difficult to reconcile with observations (Kaufman and Fraser, 1997).

This study is based on a deeper analysis of the data collected during the LBA-SMOCC project, which took place in the Amazon basin from 23 September to 18 October 2002. Andreae et al. (2004) discuss the initial results of the LBA-SMOCC experiment. Some of their main findings were as follows:

- Despite different creation mechanisms, CCN efficiency for natural biogenic and manmade pyrogenic cloud-processed aerosols is quite similar (∼70% at 1% SS). Fresh smoke has a slightly lower CCN efficiency (∼50%).
- The sensitivity of the clouds to the sub-cloud aerosol concentration increases with height and cloud vertical development. Therefore the height of precipitation onset is very sensitive to aerosol concentration. Unlike previous results, Andreae et al. (2004) did not find that this sensitivity reaches saturation at a certain aerosol concentration, probably because the pyroclouds that they have measured had stronger updrafts, which could cause greater super-saturations and further nucleation of cloud droplets.
- Although the smoke causes a negative radiative forcing at ground level, and despite the lack of evident differences in thermodynamic profile, the clouds that develop in smoky regions tend to be more vigorous and sometimes produce lightning and hail, which are otherwise scarce in the very clean environments.
- The invigorated deep convective clouds transport aerosols more efficiently from the boundary layer to higher altitudes.
- Smoky clouds can be at least partially responsible for the observed increase in upper tropospheric and stratospheric water content, because of the inhibition of rain at lower altitudes and the invigoration of the clouds that are then more likely to penetrate into the stratosphere (Rosenfeld et al., 2007).

This paper is the outcome of further analysis of this data set. It aims to give better support to some of the aforementioned findings. Moreover, this paper will concentrate on the relations between cloud water content, effective radius and cloud depth in the various aerosol regimes, highlighting and providing insights to some profound physical processes that dominate the evolution of the clouds' drop size distributions.

In Sect. 2 we will provide the background to the field campaign and the instrumentation used, including some problems that we have encountered. Section 3 will show how the vertical change in drop diameter of modal liquid water content ($D_L$) and the cloud depth required for the onset of warm rain are highly dependent on the pollution regime. Section 4 will show that CCN concentration at 0.5% SS ($CCN_{0.5\%}$) below cloud base can very well represent the important microphysical properties, such as the height for onset of warm rain. The relations obtained are tight, even when not considering cloud base updrafts, for which we have inadequate measurements. In Sect. 5 we will discuss the factors that determine the cloud droplet size distributions, as expressed by the effective radii of the cloud droplets ($r_e$). Section 6 will present the summary and conclusions.

## 2 Field campaign and instrumentation

### 2.1 Field campaign

Our work is based on the data that was collected during LBA-SMOCC (**L**arge-Scale **B**iosphere-**A**tmosphere Experiment in Amazonia – **Smo**ke, Aerosols, **C**louds, Rainfall, and **C**limate). The field campaign started at the middle of the dry season of 2002, when every day thousands of forest fires were active and released smoke to the boundary layer (BL). It went on until the beginning of the wet season the same year. The project had a ground station near the town of Ji Parana, in the state of Rondonia, where detailed measurements of aerosol physical and chemical properties and meteorological parameters were made. Two research aircraft were performing measurements during a shorter period, from 23 September to 18 October. The aircraft of the Instituto Nacional de Pesquisas Espaciais (INPE) was equipped with instruments for trace gases and aerosol measurements and was flying outside the clouds, and the other aircraft, of the Universidade Estadual do Ceará (UECE), was fitted with instruments for cloud microphysical measurements and also CCN spectra on some occasions. Ji Parana's airfield (10°52′ S 61°51′ W) served as the home base of the two aircraft, and most of the flights were conducted within few hundred km of the town, where the air was polluted for the entire duration of the aircraft campaign due to the fires in the region. In order to compare aerosols and clouds in a clean environment with the clouds in the smoky environment under relatively similar thermodynamic conditions (CAPE of the lower 5km in the range of 0–150 J/Kg), the two planes flew to the western Amazon Basin and the UECE aircraft flew subsequently to northeastern Brazil (off the coast and a little inland) as well. Both regions were not affected by the forest fires, in contrast to the region around Ji Parana (Andreae et al., 2004). In this

paper we present results that were derived primarily from the data collected by the UECE cloud microphysics aircraft.

### 2.2 Pollution regimes

Since one of the main goals of the project was to examine the effects of biomass burning aerosols on the vertical microphysical development of the clouds, the flights were made in a wide variety of aerosol loadings. Each cloud DSD (drop size distribution) vertical profile was related to the relevant CCN and CN (condensation nuclei) measurements. The closest correspondence of DSD and CCN in space and time was naturally available from the UECE CCN and DSD sensors. The INPE aircraft provided additional CN and CCN measurements in part of the cases, which were considered when the aerosols measurements had been made within 100 km and two hours from the measured clouds. In order to minimize the instrument related variability, only the UECE-measured aerosols are used quantitatively in this study.

Each cloud vertical profile was subjectively attributed to one of five aerosol regimes, quite similar to those suggested by Andreae et al. (2004), using aerosol measurements from both aircraft. We also used the ground aerosol measurement station at Fazenda Nossa Senhora (FNS) for the flights that were done in its vicinity. The flights of 23, 24, and 28 September, as well as 8, 9, 12 and 13 October were made at a distance of up to ∼100 km from FNS. Figure 1 shows $PM_{2.5}$ (particulate matter with diameter smaller than 2.5 $\mu$m) levels at FNS using a Tapered Element Oscillating Microbalance instrument ("TEOM" – Patashnick and Rupprecht, 1991, Parikh, 2000). It can be seen that the period of measurement can be divided into three shorter periods regarding the $PM_{2.5}$ levels: before 8 October when $PM_{2.5}$ levels were generally higher than 50 $\mu g\,m^{-3}$, after that and before 31 October when levels were generally around 20 to 40 $\mu g\,m^{-3}$ and afterwards when levels were very low and close to background values. Flights done on and after 8 October in the vicinity of FNS, after the passing of the extensive squall line (Fig. 2) that caused a dramatic reduction in aerosol load (Fig. 1), were therefore attributed to a cleaner regime than flights done before that. Also the Differential Mobility Particle Sizer ("DMPS" – Rissler et al., 2004) that was used during the field campaign to measure aerosol size distributions, provided similar relative changes between the days and showed a high correlation with the TEOM measurements (Rissler et al., 2006).

The aerosol-cloud microphysical regimes that we use here are the same Blue ocean, Green ocean and Pyrocloud regimes as in Andreae et al. (2004), although the measurements of the Pyroclouds are somewhat problematic due to instrumental limits, which will be discussed in Sect. 2.4. The Smoky clouds regime is referred to in this paper as Polluted regime and we also use an additional regime, the Transition regime. This regime includes the flights done either in a transition area between Polluted and Green ocean regimes, or in the period after 8 October near FNS, during the transition time to the wet season. During this time the frequency and areas of rainfall increased. This accelerated the wet deposition of the aerosols and consequently cleaned the lower troposphere, and also caused the farmers to reduce the number of new fires.

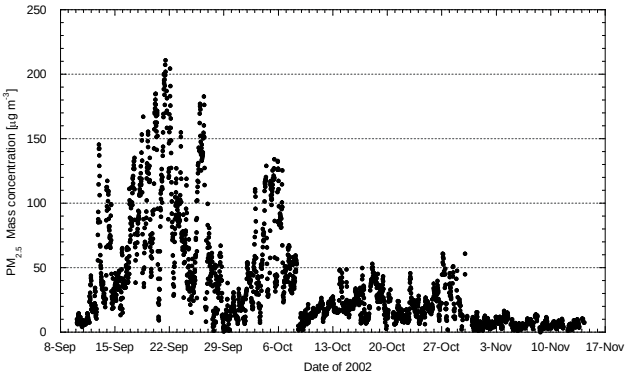


**Fig. 1.** Half-hour $PM_{2.5}$ mass concentrations at Fazenda Nossa Senhora (FNS) using a TEOM instrument for the whole period of the LBA-SMOCC field experiment. It can be seen that the entire measuring period can be roughly divided into three sub periods, ending at 8 Oct, 30 Oct and 14 Nov 2002, respectively.

The large variability in aerosol loading over the Amazon Basin makes it possible to examine the pollution-induced impacts on clouds while minimizing the synoptic or/and thermodynamic effects, which are also known to influence the microphysical development of the clouds. It can be seen in Fig. 3 that the temperature profiles do not change much from day to day and sounding to sounding, despite large distances between sounding locations and the changing seasons, except for the differences within the BL caused by: 1) the diurnal cycle (Leticia sounding from 5 October was launched at 12:00 UTC (08:00 LT) and shows the remnants of the nocturnal ground inversion) 2) the marine BL with its inversion at the top (Fortaleza sounding of 12:00 UTC 18 October) and 3) the passing of a squall line (as can be seen in Fig. 2 and as is expressed in Fig. 1) a few hours prior to the launch of the sounding from FNS (18:00 UTC 8 October), which caused cooling of the BL. But most important is the narrow range of variation in the convective available potential energy (CAPE) in the lower 5 km of the troposphere as calculated for the different soundings. Table 1 shows that CAPE values are relatively low and vary only between 0 to ∼110 $J\,kg^{-1}$ with no apparent changes between the different pollution regimes. This shows that on none of the days was the lower troposphere unstable enough to favor vigorous updrafts. Therefore we can assume that the variations in thermodynamic conditions encountered during the campaign are not the main cause for the measured variations in the microphysical parameters.

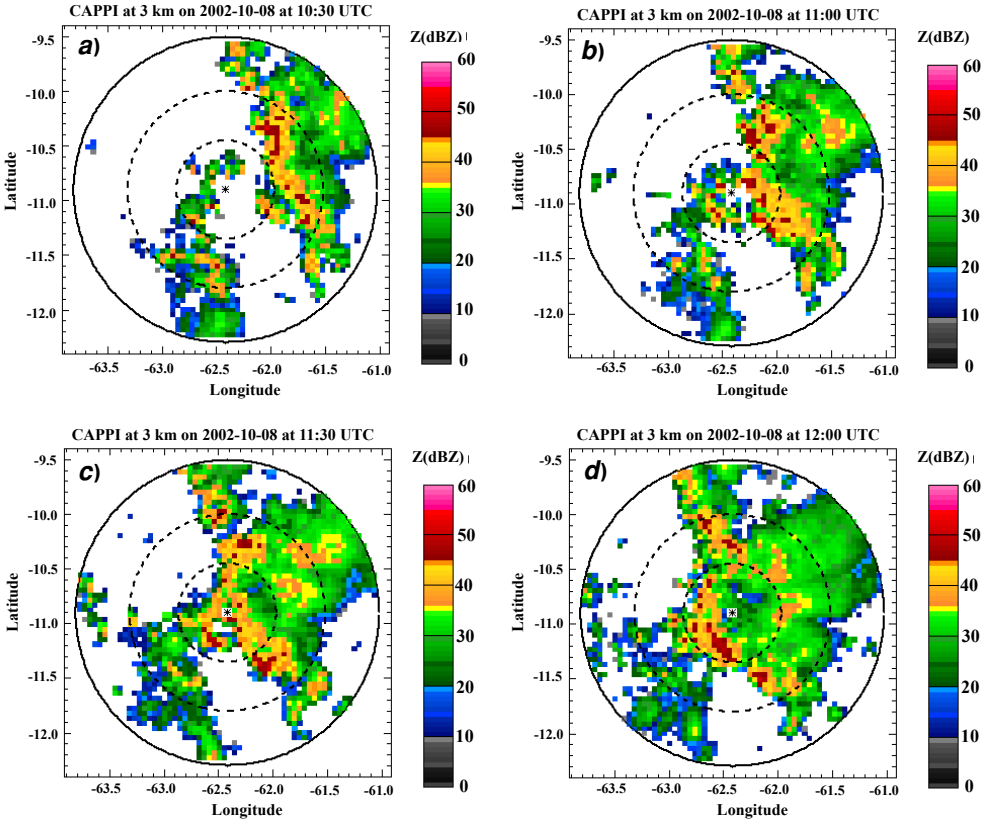


**Fig. 2.** A sequence of precipitation radar reflectivity images at a constant height of 3 km around FNS (located at the asterisk in the center of each panel) for 30 min increments, starting at 10:30 UTC 8 Oct. 2002 (panels **a** through **d**). It can be seen that a squall line, seen as the high reflectivity areas (yellow and red) located to the east of FNS at 10:30 UTC, is moving westwards and crosses FNS at around 11:30 UTC (panel c). The passing of the squall line is linked to the drastic drop in $PM_{2.5}$ concentration at the same time shown in Fig. 1.

**Table 1.** A list of the radiosondes that recorded the atmosphere's thermodynamic profile to match (in time and space) the aircraft's CCN measurements. The calculated Convective Available Potential Energy (CAPE) for the lower 5 km (the flights' height limit) of the troposphere is also shown in order to see whether the thermodynamic profiles were comparable.

| Date (of 2002) | Time | Location | CAPE (0–5 km) [J/kg] |
|---|---|---|---|
| 23 Sep | 18:00 UTC | FNS | 45 |
| 30 Sep | 18:00 UTC | FNS | 111 |
| 5 Oct | 12:00 UTC | Leticia | 86 |
| 8 Oct | 18:00 UTC | FNS | 0 |
| 9 Oct | 18:00 UTC | FNS | 21 |
| 11 Oct | 18:00 UTC | FNS | 93 |
| 12 Oct | 18:00 UTC | FNS | 53 |
| 18 Oct | 12:00 UTC | Fortaleza | 1 |

### 2.3 Instrumentation

The UECE cloud physics aircraft was equipped with the standard aircraft instruments for measuring height/pressure, temperature and flight velocity, and also had a nose weather radar. In addition, it had a GPS (Garmin) for retrieving the location of the plane as well as a dry temperature sensor (EG&G 137-C3-S3), hot wire for measuring cloud water content (CSIRO-King), forward scattering spectrometer probe for measuring cloud droplet spectra (FSSP-100 with DMT's SPP-100 package), 200X and 200Y optical array probes for measuring sizes and concentration of the hydrometeors and a cloud condensation nuclei counter (CCNC UW 83-1).

The principle of the operation of the hot wire instrument is that the cloud droplets change the electrical resistance of the hot wire by cooling it upon collision with it and evaporation. The voltage is proportional to the amount of cloud water. The error of the measurement is less than 15% (King et al., 1985).

The principle of operation, construction and the calibration method of the DH Associates static thermal-gradient CCN counter onboard the UECE cloud physics aircraft is

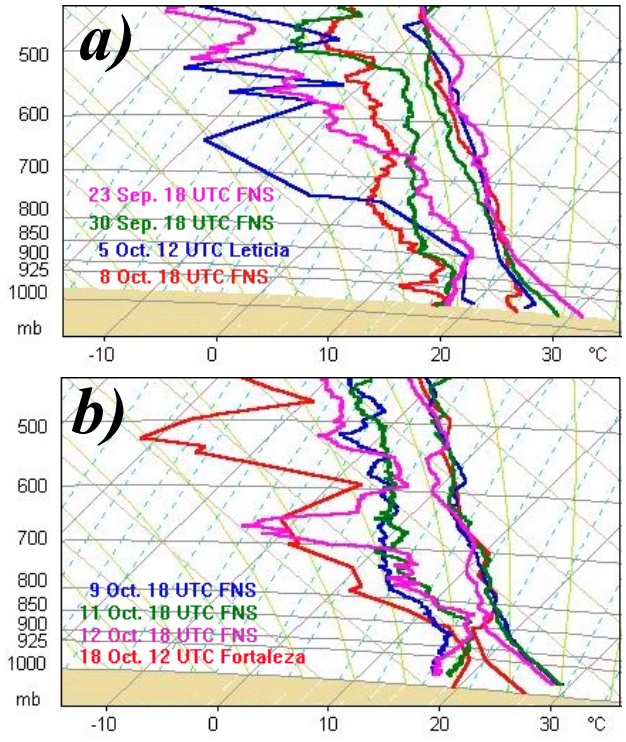


**Fig. 3.** Temperature ($T$) and dew point ($T_d$) profiles ($T_d$ is to the right of $T$ for each profile represented by a different color) on a Tephigram as derived from radiosonde measurements from all dates and near all places where below-cloud CCN measurements were done. Notice the small variance in $T$ above 850 hPa height.

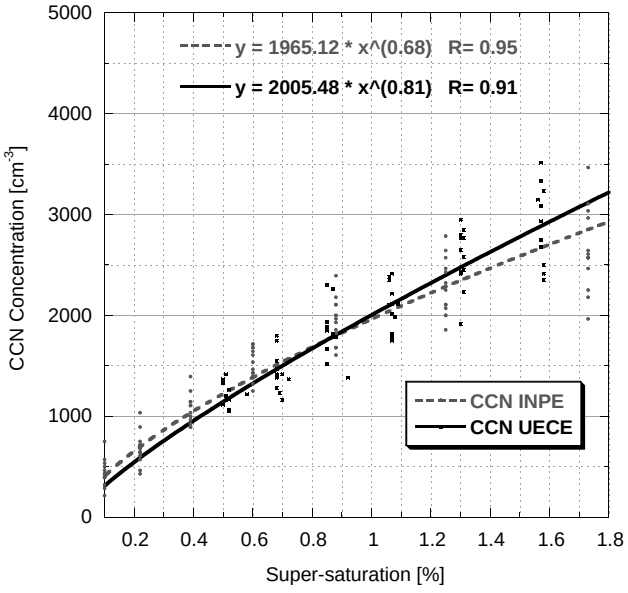


**Fig. 4.** A comparison of the CCN spectra derived from the two CCN counters on board the airplanes (INPE in grey; UECE in black) while operating in parallel on the ground on 3 Oct 2002 between 15:09 and 16:03 UTC.

thoroughly described in Oliveira and Vali (1995). Another static thermal-gradient CCN chamber was mounted on the INPE aircraft. It was calibrated with monodisperse NaCl and $(NH_4)_2SO_4$ particles in the field (Andreae et al., 2004), and its concentration measurement error is $\pm$30% at the lowest SS of 0.2% and $\pm$10% at SS of 1%. The error of the SS due to temperature fluctuations is up to $\pm$0.05% (Roberts et al., 2001). The two CCN counters were inter-compared on 3 October 2002 by running for more than an hour in parallel next to each other. Figure 4 shows that the derived CCN spectra of both instruments for the parallel measurement are comparable. The absolute concentrations and their dependence on super-saturation are quite alike because they are within the variability of the measurements.

The FSSP-100 measures the size spectrum of the cloud droplets in the range of 2 to 47 $\mu$m, based on their scattering of the laser beam that crosses the sampling volume. The size range of the droplets is divided into 30 bins with equal width of 1.5 $\mu$m each. By using the droplet spectra one can derive the cloud droplets' effective radius ($r_e$), the cloud liquid water content (LWC), and other parameters that describe the droplet size spectra.

## 2.4 Coincident droplets in the FSSP-100

Baumgardner et al. (1985) and Cooper (1988) discuss the instrumental problem in which two or more cloud droplets are present in the sampling volume of the FSSP at the same time, so that before one droplet finishes crossing the laser beam, another one is starting to cross it. As a consequence, the instrument gets a longer signal, which can either cause the rejection of both droplets or be interpreted and counted as one large droplet. In either case, there will be an underestimation in the total number of droplets, which can reach 20% when the measured droplet concentration is about 1000 cm$^{-3}$ (Baumgardner et al., 1985). This problem can also cause an artificial widening of the droplet spectrum due to the counting of several smaller droplets as one large (Cooper, 1988).

The existence of this problem implies that the droplets are distributed inhomogeneously within the cloud; otherwise this problem would not exist even in Pyroclouds, which have the largest droplet concentrations (as we will see in this section). This is because the distances between adjacent droplets would have been too large for them to cross the laser beam simultaneously (without a signal reset in between). Trying to predict a measured droplet spectrum from a known spectrum is a statistically and mathematically complex issue, and even more so the inverse calculation of the real size distribution from a measured one. For any measured distribution, there could be many different solutions for the real distributions that may have produced it. Therefore there is a large uncertainty concerning the accuracy of the measured droplet size spectra, especially in Pyroclouds, where this problem is most

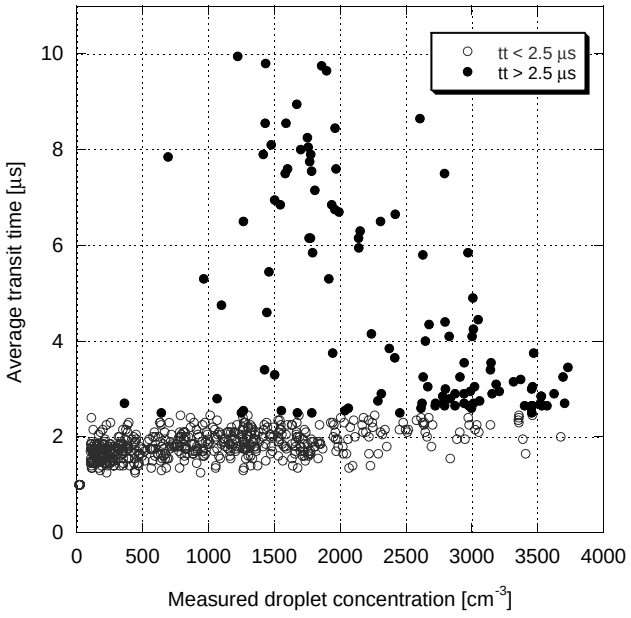


**Fig. 5.** The average droplet transit time (*tt*) across the laser beam in the FSSP-100 instrument versus the droplet concentration measured by the FSSP while flying in heavily polluted clouds around 19:00 UTC on 4 Oct 2002. Each point represents the average value along half-a-second of flight (∼40 m). Measurements with *tt* larger than 2.5 $\mu$s are suspected to be significantly affected by the "coincidence problem" and are marked with bold points, whereas measurements with a smaller *tt* are marked with circles.

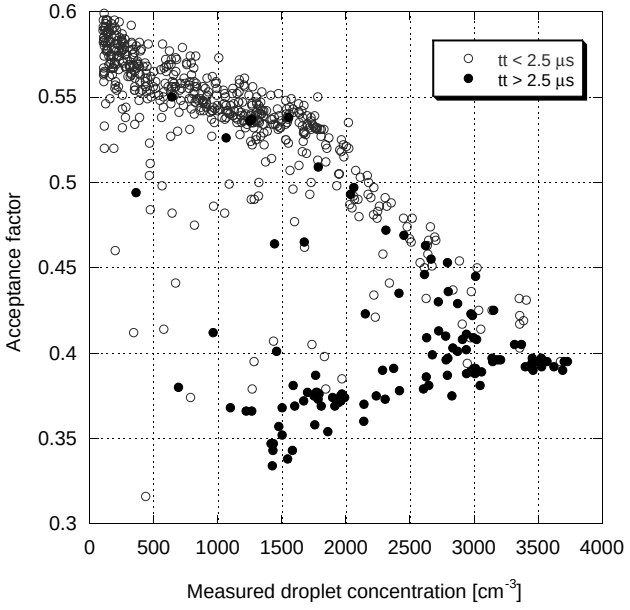


**Fig. 6.** The acceptance factor (*af* – see text for definition) as reported for each measurement versus the FSSP droplet concentration for the exact same measurements as presented in Fig. 5. Measurements with *tt* larger than 2.5 $\mu$s (see Fig. 5) are marked with bold points and show significantly smaller *af* than those with smaller *tt* (in circles).

severe because of the high aerosol concentration and strong updrafts, which have the potential to nucleate a large number of cloud droplets. In addition, the strong turbulence in the Pyroclouds causes greater inhomogeneities in drop concentrations compared to other clouds.

This instrumental problem, and the resulting underestimation in the total droplet number concentration and the artificial widening of their spectra, probably makes the Pyroclouds appear less "continental" (microphysically) compared to what they really are. Any "signal" detected by the FSSP, which will distinguish Pyroclouds from other Polluted regime clouds and show that they are more "continental", would probably be more pronounced in reality. Despite that, we chose to treat with a great deal of caution those measurements that we suspected to be influenced by coincidence, and to not base any strong conclusions upon them. Due to the complexity of this problem, which requires a comprehensive study of its own, and the uncertainty in the correction methods, we chose not to try to correct the measured droplet spectra in this work. We only show here some evidence for the existence of this problem using the FSSP's "housekeeping" variables.

The width of our FSSP's laser beam is 0.2 mm. It cannot take more than 2.5 $\mu$s for a small droplet at the average flight speed of 80 m s$^{-1}$ to cross the laser beam along its diameter. The half-second (2 Hz) average transit time for the droplets should be even less than 2.5 $\mu$s, since not all droplets cross the laser beam along its diameter. Figure 5 shows average transit times of up to 10 $\mu$s, which implies that long sequences of droplets have crossed the laser beam (at least an average of 5 droplets per sequence for a measurement with a transit time of 10 $\mu$s) causing a record of long signal by the FSSP. Those measurements with an average transit time of more than 2.5 $\mu$s are marked as bold points. All measurements shown in Fig. 5 were done during the second flight leg on 4 October 2002. When examining carefully the exact times of the flight at which most of the long average transit times were recorded, we see that the aircraft was flying inside a Pyrocloud (by using the flight reports). This does not surprise us because it is in the Pyroclouds where we expect to encounter the coincident droplets due to the very high aerosol concentration and strong updrafts, which should nucleate many of them, and where the strong turbulence should clump the droplets.

The acceptance factor, which is shown in Fig. 6, is defined as the ratio between the number of accepted strobes (a strobe is a period of time during which a scattering particle is crossing the laser beam and produces a signal) and the total strobes. The accepted strobes are analyzed and translated into the sizes of the scattering droplets. The rejection of strobes could be either because the strobe was too short, which means that the droplet had crossed the laser beam too

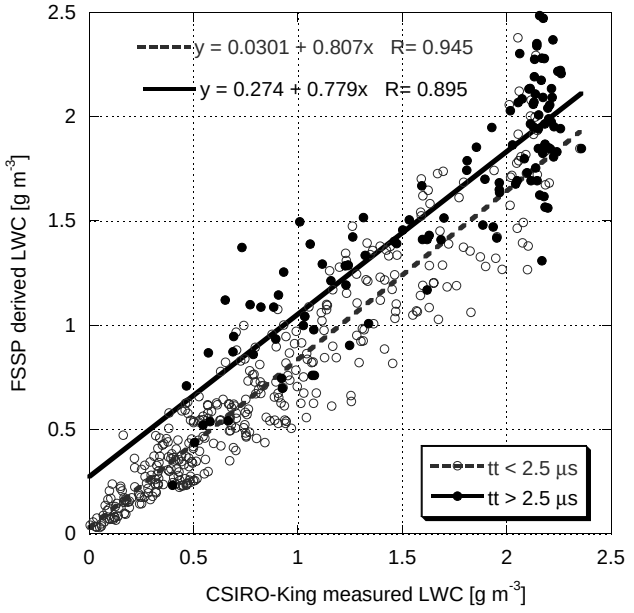


**Fig. 7.** The relation between FSSP-derived (cloud) Liquid Water Content (*LWC*) and the LWC measured by the hot-wire King probe for the same measurements as presented in Figs. 5 and 6. Again, the bold points represent the measurements with a *tt* larger than 2.5 $\mu$s. A linear regression line is shown for each group of measurements (according to their *tt*) suggesting similar slopes (p-value is 0.94 when testing for equal values) but the intercepts are slightly different (p-value is 0.024).

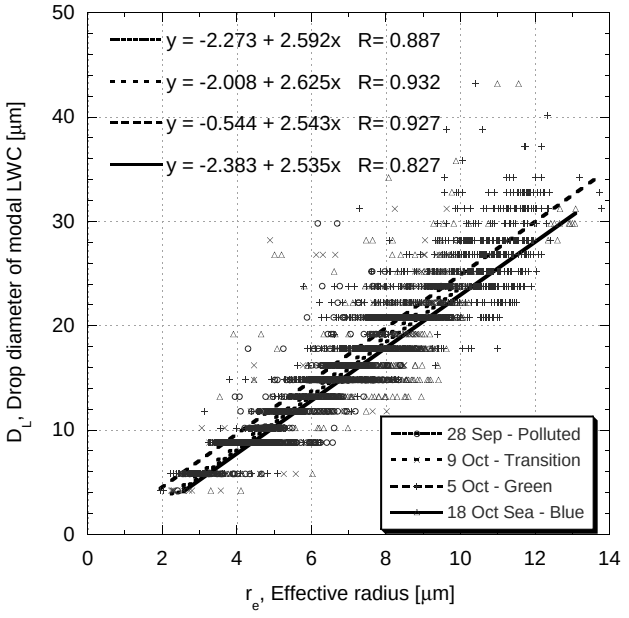


**Fig. 8.** The relation between the drop diameter of modal LWC ($D_L$) and the effective radius ($r_e$) for four representative flight legs in the different pollution regimes. Each point represents half-a-second measurement. It can be seen that there is quite a strong relation between these variables and that this relation is not strongly dependent on the pollution regime. The discrete nature of the $D_L$ values, due to the use of size-bins by the FSSP, is also noticeable.

close to its edge for the FSSP to be able calculate its size correctly, or because the droplet's pass was not in the instrument's depth of field and hence could not be analyzed correctly. According to the FSSP's operating manual, the acceptance factor, which is determined by the geometry of the instrument, should be close to 0.6. Therefore an acceptance factor of 0.4, for example, appears to suggest that we could just add 50% to the measured droplet concentration in order to get the real concentration. However, because each additional rejected strobe below the acceptance factor of $\sim$0.6 is due to at least two coincident droplets, the real concentration is probably at least double the measured one. Figure 6 shows that many of the coincidence-suspected measurements (with average transit times of more than 2.5 $\mu$s, bold points) have an acceptance factor smaller than 0.4 and therefore are probably underestimated at least by a factor of two. The apparent "folding" of the relation between acceptance factor and measured droplet concentration, at about 3500 cm$^{-3}$, implies that there are actually much greater true concentrations than the maximum of 3500 cm$^{-3}$ for the indicated lower concentrations with low acceptance factor.

The importance of the effect of the artificial broadening of the droplet spectra is shown in Fig. 7. There seems to be quite a good agreement between the CSIRO-King and the FSSP instruments regarding the cloud's LWC, despite the fact that they use completely different methods for obtaining this value. But looking at the linear trend line, we see a shift between the coincidence-suspected measurements and the other measurements. For a given LWC measured by the King hot wire (which is not susceptible to the coincidence problem but on the other hand saturates at $\sim$2.3 g m$^{-3}$) the FSSP-derived LWC shows slightly larger values in general, despite the underestimation in the total droplet concentration. The only reasonable explanation for that is that there is an artificial widening of the droplet spectra, which adds more cloud water content than the loss due to the underestimation in droplet number, probably because the LWC is strongly dependent on the size of the droplets (by the power of three), so a small artificial addition of large droplets gives more water mass than the loss of many small droplets.

## 3 Modal drop size and onset of rain

Andreae et al. (2004) have shown how the size distributions of cloud droplets change with the vertical development of the clouds. They have done so by choosing one representative flight for each of their pollution regimes. Although this kind of presentation shows the whole size spectra, it is difficult to compare the change with height for different flights or/and pollution regimes. In order to facilitate this comparison, we

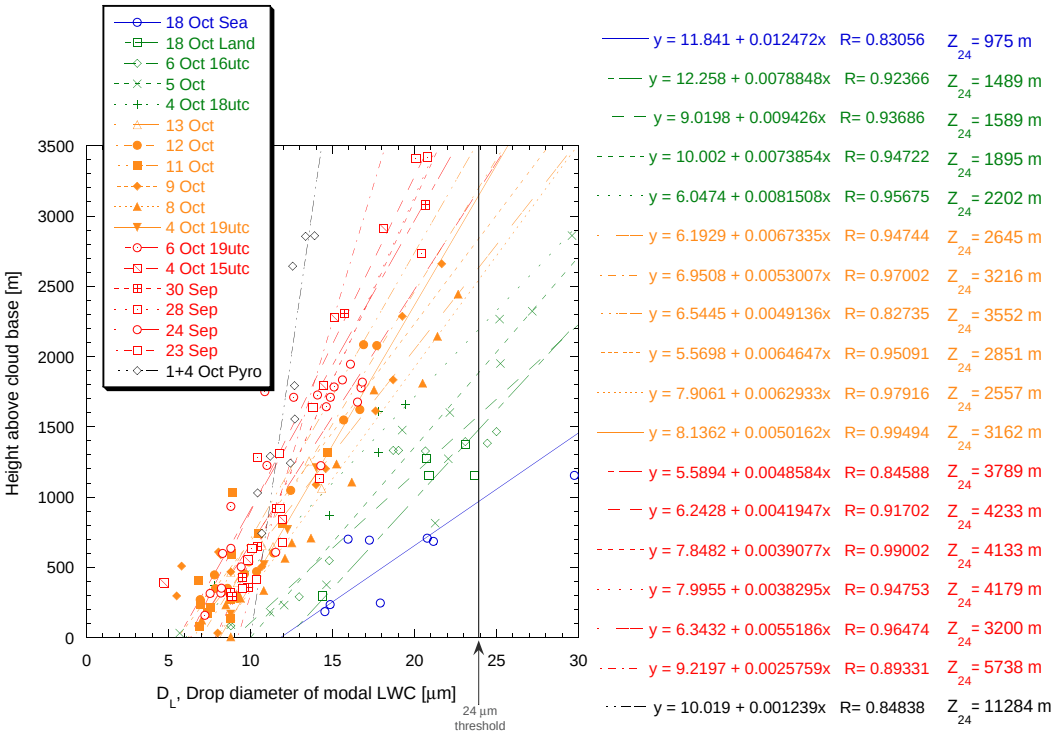


**Fig. 9.** The growth of $D_L$ with cloud depth for all flights that included a vertical cloud profile of at least 1 km depth. Each point represents the averaged $D_L$ for one horizontal penetration at a certain height. The color scheme is based on the pollution regime in the following way: in blue are Blue Ocean measurements, in green – Green Ocean, in orange – Transition Regime, in red – Polluted Regime and in black – Pyroclouds. Each profile was named after its date and if necessary, its time and additional self-explanatory information. The order of the profiles' appearance in the legend corresponds to the order of the equations of the best-fit linear regressions shown to the right. The 24 $\mu$m threshold for the onset of warm rain is marked on the figure. The cloud depth at which $D_L$ crosses this threshold for each profile – $Z_{24}$, is shown at the extreme right. It can be seen that in the more polluted regimes, the clouds need to have a larger vertical extent in order for $D_L$ to reach the 24 $\mu$m warm rain threshold, compared to the clouds in the cleaner regimes.

have chosen here to characterize the whole spectrum by one single parameter: the modal diameter of the droplet size distribution (by mass), $D_L$. This parameter is strongly correlated with the droplet effective radius ($R$=0.92), and its relation to $r_e$ is not noticeably dependent on the pollution regime (see Fig. 8). $D_L$ is also less affected by the coincidence problem in comparison to $r_e$ and LWC, which are usually overestimated because of the artificial widening of the spectra (stretching the tail of the distribution does not change its mode), or the total droplet concentration, which is underestimated. Figure 9 shows how $D_L$ changes with cloud depth (to account for the differences in cloud base elevation) for all flights that included a vertical profile of at least 1000 m in depth. The color scheme represents the pollution regime, so that warmer colors depict more polluted environments. The vertical line at a droplet diameter of 24 $\mu$m is the threshold $D_L$ for the onset of warm precipitation, as it normally coincided with the appearance of echoes on the aircraft radar and visible impacts of raindrops on the windshield (Andreae et al., 2004). Because the measurements in the Transition regime, Polluted regime and Pyroclouds did not extend high enough in the cloud to reach this threshold, we have extrapolated the (good) linear fit in order to get an estimated value for $Z_{24}$, which is the cloud depth at which $D_L$ crosses the 24 $\mu$m threshold. It can be clearly seen that clouds in the more polluted regimes need to reach larger depths in order to produce rain by warm processes. If we add the average cloud base height (about 1500 m) in the Polluted regime to the cloud depth required for warm rain to start in these clouds (more than 4000 m), we reach heights where the temperature is well below freezing and hence the raindrops produced by coalescence readily freeze and continue to grow as graupel and hail.

The profile of the Pyrocloud in Fig. 9 is only presented for comparison with the rest of the profiles. The values of the parameters shown have a large uncertainty because of the coincidence problem and the fact that the profile was constructed by using two different flights so the profile would be deep enough. Furthermore, it is difficult to determine accurately the cloud base height, and also the updrafts at the Pyroclouds' bases were probably significantly stronger than the updrafts in the other cases, due to the heat released

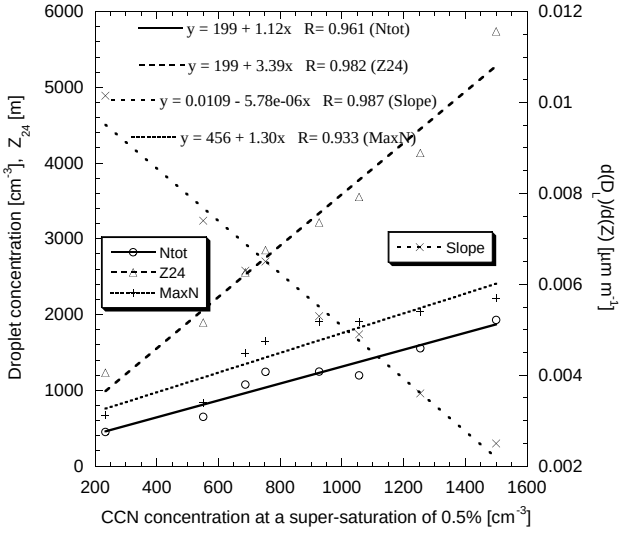


**Fig. 10.** The relations between CCN concentration at 0.5% SS and four FSSP derived microphysical parameters: $N_{\mathrm{tot}}$ – the average droplet concentration, $Z_{24}$ – the required cloud depth for the onset of warm rain, max$N$ – averaged maximum droplet concentration and Slope – the derivative of $D_L$ with height. Each point represents one complete profile, which is based on at least five cloud penetrations at a range of heights of more than 1 km. Clear linear relations between these independent measurements are seen for all variables.

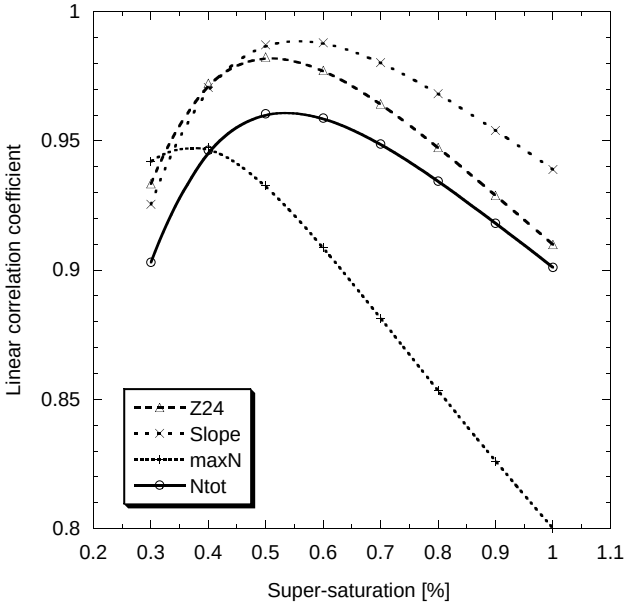


**Fig. 11.** The linear correlation coefficients between each microphysical parameter shown in Fig. 10 and the interpolated CCN concentration at different super-saturations (SS) that was based on the measurements of the CCNC. It can be seen that the correlation coefficients peak at SS of 0.5–0.6% for all variables but max$N$.

by the fire. The stronger updrafts could have caused higher super-saturations at cloud base, which would have nucleated a larger fraction of the CN into cloud droplets that would have then grown slower by diffusion and coalescence.

## 4 CCN measurements

The variability in aerosol concentration during the burning season in the BL is quite large due to the heterogeneous spatial distribution of the fires and the scattered rain events, which can reduce the aerosol concentration locally. Therefore it is not very useful to compare cloud microphysical properties and aerosol measurements done on/from the ground or by the other aircraft, unless it was measuring directly below the cloud analyzed microphysically. For the same reason it is difficult to compare the development of a specific cloud to the aerosol load or aerosol optical depth derived from satellite data, which have a high uncertainty over land, rarely match in time and space, and retrieve a value for the whole column of air. The best way to have some independent and more objective measurements of the aerosol properties and their effects on the microphysical development of the clouds in this heterogeneous area is to measure the aerosols below the bases of the penetrated clouds. For this purpose, a CCN counter was mounted on the UECE cloud physics aircraft. It was unfortunately not used for every cloud vertical profile, but we did obtain eight coupled measurements (below cloud and in cloud), which Fig. 10 is based on. In this figure we can see how $\mathrm{CCN}_{0.5\%}$ (derived from the best fit power equation for the whole measured CCN spectra) below cloud base is related to the microphysical properties of the same cloud, derived from the FSSP-100 measurements. The Pyroclouds are not included, but there still is a large span of CCN concentrations.

We have used linear fits in Fig. 10, not necessarily because of physical principles, but because it is the simplest model and still it shows a surprisingly good fit for all variables. The SS value of 0.5% was used because it was in the range of all measurements so that no extrapolation was needed, and because it is a typical value of SS near cloud base. This is evident by the observation that the average droplet concentrations that were measured ($N_{\mathrm{tot}}$) are quite similar to the CCN concentration at that SS. Figure 11 also supports this choice by showing that the strength of the linear relations of CCN concentrations with all the variables shown in Fig. 10 indeed peaks at around SS=0.5%.

The deviations from the relation shown between $\mathrm{CCN}_{0.5\%}$ and average droplet concentration (Fig. 10) can be, among other things, the consequence of slightly different SS at the cloud bases. But the finding that the variance in $Z_{24}$ is slightly better explained by $\mathrm{CCN}_{0.5\%}$ than by average droplet concentration (96.5% compared to 94.4%, the latter not shown here), which should already take the differences in the updrafts into account, suggests that the updrafts near the bases of the different clouds were comparable, as already

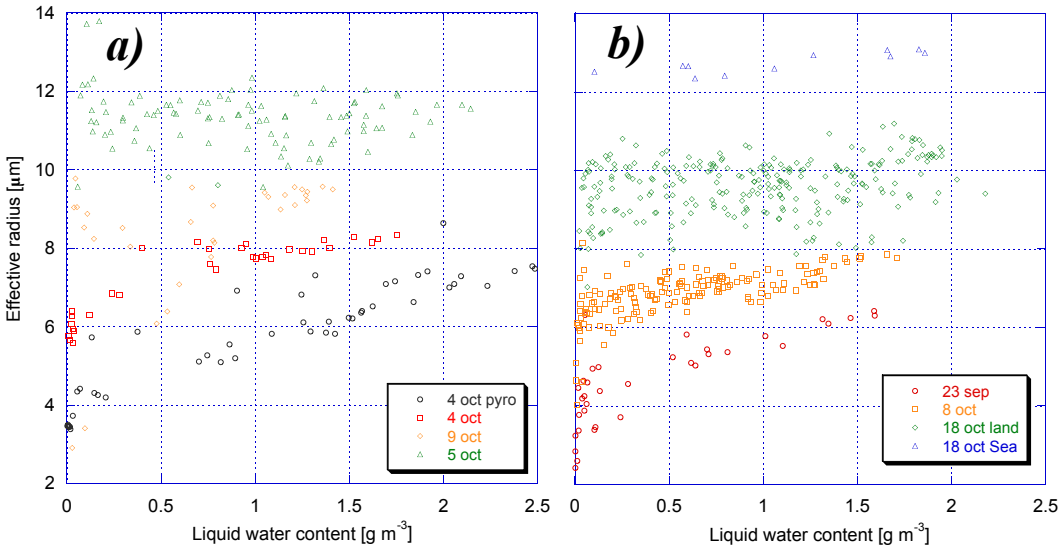


**Fig. 12.** The dependence of the effective radius ($r_e$) on the Liquid Water Content (LWC) for the different pollution regimes (each represented by one flight leg) at a nearly constant cloud depth of 2700 m in panel **(a)** and of 1200 m in panel **(b)**. Each point represents one measurement averaged on circa 40 m of horizontal flight. The color scheme is the same as in Fig. 9. $r_e$ shows only a small variance compared to LWC and its value is higher for the cleaner regimes when looking at a nearly constant height.

suggested by the small values of CAPE in the lower 5 km of the troposphere (Table 1). The very strong relation between CCN concentration and $Z_{24}$ suggests that it is not necessary to know the updraft velocities at cloud base (which were not measured objectively) in order to determine the height for the onset of warm precipitation (within $\pm$300 m), at least for the wide variety of conditions that encompass the transition from the polluted to clean environments and from the dry to the wet season in the western Amazon. It will be interesting to see if this relation extends to other seasons or regions.

Figure 10 also shows that the CCN concentration correlates strongly with the derivative of $D_L$ with height and with max$N$, which is defined as the average of the maximum droplet concentrations measured during each penetration within the same profile/cloud. This parameter is more sensitive than $N_{\text{tot}}$ to the exact path of the plane in the cloud (whether the plane has passed through the core of the cloud or just nearby) and to the coincidence problem. Moreover, each maximum value is the average along a $\sim$40 m path (because of flight speed and measurement frequency), so the retrieved value does not necessarily correspond to the real maximum value in the same way for each penetration. These reasons could cause the smaller correlation coefficients of max$N$ with CCN concentrations compared to $N_{\text{tot}}$, as can be seen in Fig. 11 for all levels of SS above 0.4%. They can also be a part of the explanation for the shift in the peak of the curve of max$N$ in the same figure. Therefore we consider $N_{\text{tot}}$ as more representative of cloud properties than max$N$. The rate of change in $D_L$ with height (Slope in Figs. 10 and 11) is strongly linked to $Z_{24}$ and shows a very high correlation coefficient as well.

## 5 The effective radius

The cloud droplet effective radius ($r_e$) is often used as a representative parameter for the droplet size spectra. It is also the only droplet size dependent parameter that can be retrieved from the analysis of satellite data, due to considerations of radiative transfer theory. It can also be derived from the measured droplet spectra. Because of its strong link to cloud mediated radiative processes, we wanted to find out which are the factors that determine the value of $r_e$ and to what extent. It has already been shown that clouds in polluted regions tend to have smaller $r_e$ compared to similar clouds in cleaner environments (e.g., Kaufman and Fraser, 1997; Rosenfeld and Lensky, 1998; Rosenfeld, 2000). It is also known that $r_e$ below the precipitation forming level increases with cloud depth. As the cloud droplets travel to colder temperatures higher in the cloud, the excess water vapor can condense on them and they can also coalesce into larger droplets, both of which will increase $r_e$. Therefore it is important to separate the cloud depth effects from the aerosol load effects on $r_e$. Figure 12 does so by presenting $r_e$ (measured at 2 Hz) for all different pollution regimes, at two almost constant cloud depths (2700 m in panel *a* and 1200 m in panel *b*). It can be clearly seen that for a given cloud depth, the cleaner the environment the larger are the effective radii. It can also be seen that for a given environment and height, $r_e$ is very robust, i.e., it does not change much (within a range of $\sim$2 $\mu$m, except for Pyroclouds where falsely large effective radii are expected due to coincident droplets in the FSSP) regardless of the measured LWC or adiabatic fraction. The adiabatic fraction (ratio between measured LWC and adiabatic

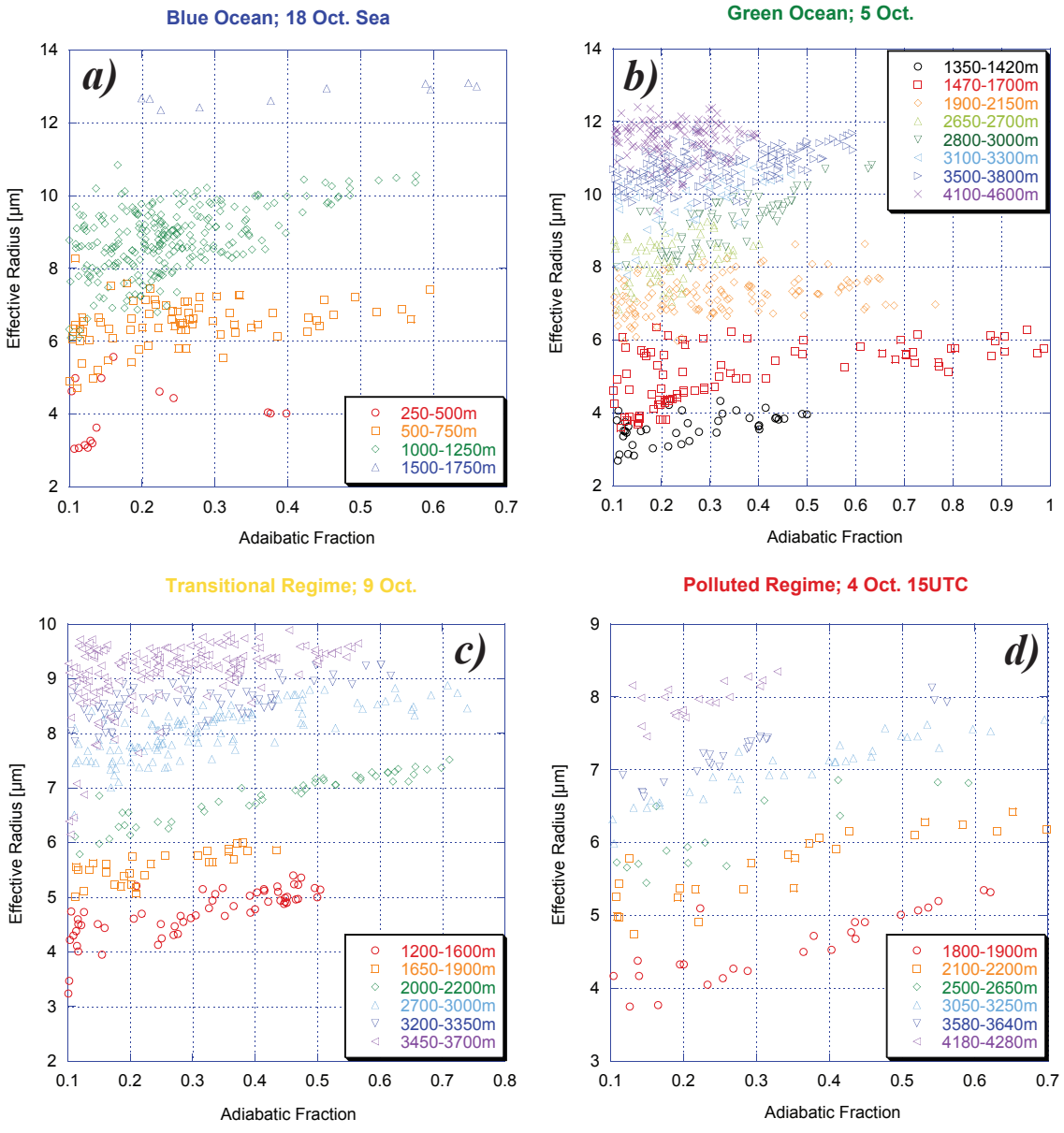


**Fig. 13.** The dependence of $r_e$ on the adiabatic fraction for all measurements done in the same flight leg, grouped by the different heights (above sea level). Panels **(a)**, **(b)**, **(c)** and **(d)** display the measurements of representative flight legs for the Blue Ocean, Green Ocean, Transition and Polluted regimes, respectively. Each point represents one measurement averaged on circa 40 m of horizontal flight. It can be seen that within each group of heights, $r_e$ is quite robust and also that its value is generally increasing with increasing height, for all regimes.

maximum theoretical water content) is determined by the degree of cloud dilution due to entrainment of droplet-free air from the surroundings of the cloud. This, and the fact that the measurements were not limited to only one cloud in each leg, strengthen one of the basic assumptions on which satellite data analysis relies, which is the ability to look at different cloud tops (at different heights) in the same region and regard their effective radii as if they were measured inside one well developed cloud, revealing the microphysical processes that take place in the cloud (Rosenfeld and Lensky, 1998).

Figure 13 examines each regime separately and shows the changes in $r_e$ with cloud depth and with the liquid water content (LWC) normalized to adiabatic fraction. Each cloud depth interval in Fig. 13 shows a relatively small variability in $r_e$, as seen in Fig. 12. In addition, the value of $r_e$ is constantly increasing with height for each aerosol regime. Furthermore, careful examination of Figs. 12 and 13 shows that $r_e$ depends less on LWC for larger values of $r_e$. The dependence vanishes altogether when $r_e$ exceeds $\sim$10 $\mu$m, which is equivalent to $D_L$=24 $\mu$m (see Fig. 8), the threshold for onset

of warm rain processes. This threshold for $r_e$ is smaller by 2–4 $\mu$m than the threshold reported by Rosenfeld and Gutman (1994) based on the analysis of satellite images, due to the ability to separate the precipitation particles, which increase $r_e$, from the cloud droplets in in situ measurements.

We suggest that $r_e$ becomes somewhat smaller with reduced LWC for clouds with small drops because such drops grow mainly by condensation. Entrainment of dry air from the surroundings of the cloud causes partial evaporation of the droplets and therefore decreases LWC and $r_e$. The decrease of $r_e$ with LWC is relatively small because the smaller droplets evaporate first, leaving the largest drops in the cloud.

We suggest the following explanation for the lack of sensitivity of $r_e$ to LWC for clouds with drops that are sufficiently large for significant coalescence, i.e., for $r_e > \sim 10\,\mu$m: The maturation of the cloud is associated with the opposing processes of droplet evaporation and coalescence, which nearly cancel each other leaving the cloud drops with the same $r_e$ with maturation. These effects are evident in Figs. 12 and 13.

As far as we know, this gradual change in the relation between $r_e$ and LWC has not been documented before. Previous studies in clean maritime stratus and stratocumulus clouds have shown that $r_e$ is not dependent on LWC (Brenguier et al., 2000; Gerber, 1996; Gerber et al., 2001). These authors, as well as Baker et al. (1980), explain this finding with the inhomogeneous mixing theory, which claims that droplet evaporation is a very quick process compared to turbulent mixing, so that when undersaturated air is being entrained, it causes instant droplet evaporation. When the air reaches saturation, further mixing will only dilute the cloud and hence cause a decrease in droplet concentration and LWC, but will have no effect on droplet size spectra and $r_e$. In other words, this theory suggests that the cloud is made up of micro-parcels with a variety of LWC and droplet numbers according to the history of their mixing, but with a rather constant effective radius.

Blyth and Latham (1991) have also observed independence of $r_e$ on LWC, but in clean cumulus clouds in Montana. Although it is possible to notice it in their published results, they do not mention that there seems to be a small $r_e$ dependency on LWC when $r_e$ is smaller than $\sim 10\,\mu$m. On the other hand, Reid et al. (1999) have found a positive correlation between $r_e$ and LWC, such as we have seen here for the smaller values of $r_e$. Their measurements were, however, confined to "non-precipitating cumulus clouds" and they did not take the cloud depth factor into account, and therefore could not see its effect on the $r_e$-LWC relation. These findings somewhat contradict the inhomogeneous mixing theory, because $r_e$ is decreasing slightly with decreasing LWC and does not remain constant. Furthermore, Reid et al. (1999) came to the conclusion that the effective radii are not dependent on the level of aerosol loading beyond a threshold of 3000 cm$^{-3}$ (accumulation mode, $>100$ nm), but only on LWC. We did not see this saturation in the aerosol effect, despite flying in Pyroclouds where aerosol concentrations are larger by an order of magnitude (Andreae et al., 2004). The effective radii measured in Pyroclouds were smaller than in other polluted clouds (Fig. 12a) although there is an overestimation in $r_e$ due to coincidence. The same can also be seen in Fig. 9 by the smaller $D_L$ (which is not significantly affected by coincidence) at greater cloud depths in Pyroclouds.

The apparent reason for Reid et al. (1999) not being able to detect a different $r_e$-LWC relation between the Pyrocloud ("Fumulus" in their paper) and other, less polluted clouds is that they did not measure high enough in the cloud (their maximum measured LWC was 1.5 g m$^{-3}$ which is typical for a cloud depth of $\sim$1000 m). At small cloud depths it is impossible to unambiguously identify differences in $r_e$ or in $D_L$ between Pyrocloud, Polluted and Transition regimes, because small changes of depth induce large changes in $r_e$. Just above cloud base even Green ocean clouds have similar values of $D_L$ and $r_e$ as the more polluted clouds at slightly greater depth. It is possible to detect significant differences between the pollution regimes only by measuring at greater cloud depths, as indicated by the divergence of the data with height in Figs. 9 and 14. In addition to that, Fig. 14 also shows how the standard deviation of $r_e$ for all regimes is quite small, despite including all adiabatic fractions, and that the standard deviations of the different regimes do not overlap at cloud depths greater than $\sim$1500 m. Once again, this shows that, for a given height or temperature, $r_e$ is robust enough to be used in remote sensing to give information on aerosol-cloud interactions. Similar robust relations between aircraft measured $r_e$ and height about convective cloud base were documented previously in Indonesia by Rosenfeld and Lensky (1998).

Another potentially important factor that might affect the $r_e$-LWC relation is the sampling frequency, because the sampling frequency determines the horizontal scale of the measurements. The micro-parcel interactions with each other as well as the turbulence scales may not be resolved due to the inevitable spatial averaging caused by the limited sampling frequency. Therefore higher sampling frequency is needed in order to separate the physical processes effects on $r_e$-LWC relation from the small scale mixing interactions.

## 6 Summary and conclusions

In this study we have analyzed in detail the in situ measurements made inside convective clouds during the LBA-SMOCC project in the Amazon Basin in the late dry season 2002. The main goals of this work were 1) to strengthen the conclusions of previous studies regarding the aerosol effects on cloud microphysical development and 2) to determine how $r_e$, as a representative parameter of the cloud droplet spectra, is affected by other factors.

To accomplish the first goal, each of the 32 flight legs has been assigned to one of five aerosol/cloud microphysical

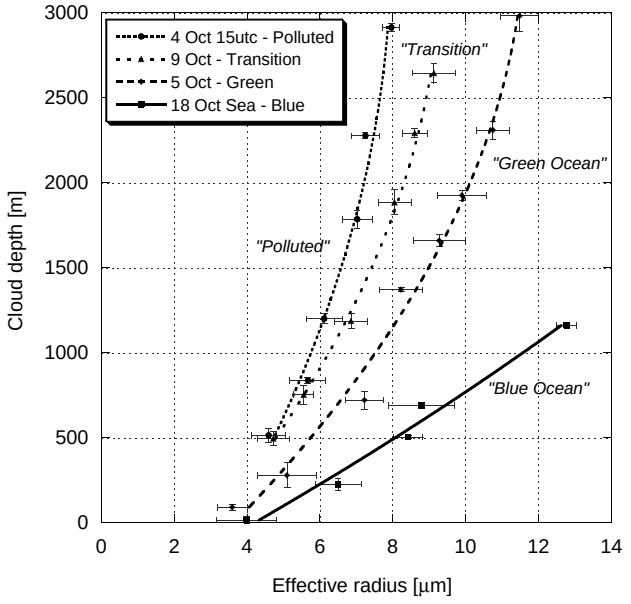


**Fig. 14.** The growth of $r_e$ with cloud depth for different flight legs from the different regimes. Each point shows the average $r_e$ and the average cloud depth based on the altitude-grouping and the data shown in Fig. 13 for all adiabatic fractions. The standard deviations for both $r_e$ and the cloud depth are shown as well, in order to see whether there are significant differences between the different regimes' $r_e$ profiles and whether their standard deviations overlap. The standard deviations for the cloud depth are quite small because of the horizontal cloud-penetrations at discrete heights. It can be seen that all four profiles start with $r_e$ of $\sim$4 $\mu$m, but then there is a divergence further up in the cloud, so that at cloud depths of 1500 m and above there is no overlap in the standard deviations of $r_e$, despite not using all adiabatic fractions.

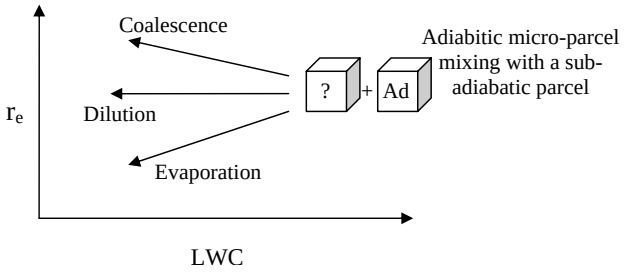


**Fig. 15.** Schematic illustration of the probable effects of the evaporation, dilution and coalescence processes on the $r_e$-LWC relation when an adiabatic parcel mixes with another sub-adiabatic parcel. The box marked with "Ad" represents the adiabatic parcel and its location on the $r_e$-LWC plane is meaningful, while the box marked with a question mark represents the sub-adiabatic parcel and its location on the plane is variable although its LWC has to be smaller than the adiabatic parcel (when there are no falling-from-above precipitation particles). The final location of the newly mixed parcel on the $r_e$-LWC plane will be determined by the relative importance of the above mentioned processes.

regimes, because in most cases no adequate method for retrieving aerosol data below cloud base was available. Despite a significant coincidence problem in the FSSP-100, especially during Pyrocloud penetrations, significant differences in the rate of $D_L$ growth with cloud depth were observed between the various aerosol regimes.

Because of the slow increase in $D_L$ with cloud depth in the polluted clouds, they did not reach the 24 $\mu$m threshold for the onset of warm rain at temperatures above freezing. Therefore, the droplets were too small to rain out at lower levels and could be transported to heights where they were likely to freeze and continue growing as graupel or hail. The relatively small droplets in the polluted cases, which have a smaller chance of freezing, could provide large amounts of supercooled water, which could encourage the formation of hail and lightning as suggested by Andreae et al. (2004). In addition, the separation between Polluted regime and Transition regime showed to be useful because the Transition regime clouds that were fed by the less polluted BL clearly showed a less "continental" microphysical behavior.

Moreover, the CCN concentrations below cloud base, in particular $CCN_{0.5\%}$, were found to be very good predictors for the cloud depth required for onset of warm rain, leaving only a secondary role for the updraft velocity at cloud base in the sampled clouds. On average, the addition of 100 $CCN_{0.5\%}$ cm$^{-3}$ would increase the cloud depth required for the onset of warm rain by $\sim$350 m. It will be interesting to see whether this strong relation extends to other seasons or/and locations.

Regarding the second goal of this study, it was shown that $r_e$ depends first of all on depth above cloud base, and the rate of its growth with the cloud depth depends on the aerosols that feed into the cloud base. The effective droplet radius at cloud base is always very small, but it strongly diverges with cloud depth for the various aerosol regimes.

It was also apparent that for a given height and cloud, $r_e$ is somewhat dependent on the liquid water content, which is limited by the adiabatic water and is controlled by the degree of the cloud's mixing with entrained air. According to the measurements, this dependence seems to be less and less evident as $r_e$ increases, until it is not noticeable when $r_e$ reaches $\sim$10 $\mu$m. In previous studies only the "limits" of this dependence have been discussed and not the gradual change that is reported here. Most likely, we were able to detect this gradual change because of the relatively deep vertical profiles that our results are based upon. To explain this gradual change in the dependence of $r_e$ on LWC in deep convective clouds, we propose the following hypothesis, which can also explain the observations reported in previous studies and in different types of clouds:

The maximum LWC is limited by the adiabatic water content ($L_{ad}$) for any given height. A cloud parcel that has started to rise from cloud base and reached its height without

mixing with a diluted cloud parcel or dry ambient air will have the adiabatic water content and an effective droplet radius depending on the aerosol properties that it was formed from and the conditions at cloud base. Assuming no coalescence or evaporation of the droplets, $r_e$ should be proportional to $r_{ad}$, which is the "adiabatic radius", and in case of monodisperse droplets it should equal:

$$r_e = r_{ad} = \left(\frac{3}{4}\pi\rho_w\right)^{\frac{1}{3}} \left(\frac{L_{ad}}{N_{ad}}\right)^{\frac{1}{3}} \quad \text{(Blyth and Latham, 1991)}$$

Where $\rho_w$ is the water density and $N_{ad}$ is the number of droplets in the adiabatic parcel.

When this adiabatic parcel eventually mixes with a sub-adiabatic parcel (or with dry ambient air as the extreme case) the LWC will inevitably decrease but the new value of $r_e$ will be determined by the relative weight of three processes: evaporation, dilution and coalescence (see Fig. 15 for illustration). If the entrained parcel is under-saturated, the droplets will partially evaporate and $r_e$ will decrease. Because the smaller droplets evaporate faster, they will evaporate completely and leave a residual population of large drops that decreased only slightly in size. Therefore, $r_e$ is reduced only slightly with decreasing adiabatic fraction (see Fig. 13). If the entrained air is also saturated, there will only be cloud dilution and $r_e$ will remain unchanged. When $r_e$ is sufficiently large to be affected significantly by droplet coalescence ($r_e > \sim 10\,\mu$m), the selective evaporation of the smaller drops along with the continued coalescence of the large drops cancel each other out, leading to stability of $r_e$ with the adiabatic fraction. The effective radius could even increase with maturation and dilution of a cloud with very large droplets and strong coalescence.

According to this hypothesis, a horizontally extended shallow stratocumulus that is not affected much by entrainment of dry environmental air, except for at its top and boundaries will be mostly adiabatic and there will not be large variations in LWC or $r_e$. If a bubble of dry air is entrained by this cloud, it will quickly become saturated and then will dilute the adiabatic cloud and introduce larger variations in LWC and droplet concentration while leaving $r_e$ practically unchanged. Such a behavior was documented by Brenguier (2000) and Gerber (1996). Their observations as well as the high frequency (1 kHz) measurements done by Gerber et al. (2001) in clean cumulus clouds, contradict the homogeneous mixing theory which expects the cloud to be uniform (and therefore $r_e$ must also remain constant for a given height). The aforementioned studies claimed that the mixing in the clouds is inhomogeneous, i.e., that there are adiabatic micro parcels that are either evaporated instantly and completely, or only diluted upon mixing with entrained air and therefore $r_e$ will remain constant and not be dependent on LWC as long as the droplets do not evaporate completely.

The decrease in $r_e$ with mixing in cumulus clouds, shown in this paper and by Reid et al. (1999), who have measured cumulus clouds with $r_e$ of up to $\sim 9\,\mu$m, implies that the micro parcel theory is too extreme assuming instant evaporation (compared to the time of turbulent mixing), since the observed effect of the mixing is a small reduction in $r_e$ caused by the partial evaporation of the droplets. When coalescence becomes more effective, it starts compensating for the reduction of $r_e$ due to evaporation. When $r_e$ reaches $\sim 10\,\mu$m, coalescence becomes sufficiently active to completely balance the effect of the evaporation on $r_e$. In cumulus clouds, the dilution effect has an insignificant role compared to the evaporation and the coalescence effects and compared to its role in stratiform clouds. The hypothesis proposed here is potentially very useful, as it can provide a comprehensive and general description of the $r_e$-LWC relationship, but since it is based on a relatively small number of cases, it is essential to validate it with more cases from different regions, other cloud types and using higher sampling frequencies, in order to learn how the small scale mixing processes affect this relationship.

*Acknowledgements.* This work was carried out within the frame work of the Smoke, Aerosols, Clouds, Rainfall, and Climate (SMOCC) project, a European contribution to the Large-Scale Biosphere-Atmosphere Experiment in Amazonia (LBA). It was financially supported by the Environmental and Climate Program of the European Commission (contract No. EVK2-CT-2001-00110 SMOCC), the Max Planck Society (MPG), the Fundação de Amparo à Pesquisa do Estado de São Paulo, and the Conselho Nacional de Desenvolvimento Científico (Instituto do Milênio LBA). We thank all members of the LBA-SMOCC and LBA-RACCI Science Teams for their support during the field campaign, especially A. C. Ribeiro, M. A. L. Moura, and J. von Jouanne. The authors would also like to thank M. Avissar and O. Burstein for the help with the construction of the thermodynamic charts, and C. Morales for the radar images.

Edited by: S. Fuzzi

## References

Andreae, M. O., Rosenfeld, D., Artaxo, P., Costa, A. A., Frank, G. P., Longo, K. M., and Silva-Dias, M. A. F.: Smoking Rain Clouds over the Amazon, Science, 303, 1337–1342, 2004.

Baker, M. B., Corbin, R. G., and Latham, J.: The influence of entrainment on the evolution of cloud droplet spectra: I. A model of inhomogeneous mixing, Q. J. Roy. Meteor. Soc., 106(449), 581–598, 1980.

Baumgardner, D., Strapp, W., and Dye, J. E.: Evaluation of the Forward Scattering Spectrometer Probe. Part II: Corrections for coincidence and dead-time losses, J. Atmos. Ocean. Tech., 2, 626–632, 1985.

Blyth, A. M. and Latham, J.: Notes and Correspondence – A climatological Parameterization for Cumulus Clouds, J. Atmos. Sci., 41, 2376–2371, 1991.

Brenguier, J. L., Pawlowska, H., Schüller, L., Preusker, R., Fischer, J., and Fauquart, Y.: Radiative Properties of Boundary Layer Clouds: Droplet Effective Radius versus Number Concentration, J. Atmos. Sci., 57, 803–821, 2000.

Coakley Jr., J. A., Bernstein, R. L., and Durkee, P. A.: Effect of ship-stack effluents on cloud reflectivity, Science, 237, 1020-1022, 1987.

Cooper, W. A.: Effects of Coincidende on Measurements with a Forwards Scattering Spectrometer Probe, J. Atmos. Ocean. Tech., 5, 823–832, 1988.

Costa, A. A., Oliveira, C. J., Oliveira, J. C. P., and Sampaio, A. J. C.: Microphysical Observations of Warm Cumulus Clouds in Ceará, Brazil, Atmos. Res., 54, 167–199, 2000.

Eagan, R. C., Hobbs, P. V., and Radke, L. F.: Measurements of Cloud Condensation Nuclei and Cloud Droplet Size Distributions in the Vicinity of Forest Fires, J. Appl. Meteorol., 13(5), 553–557, 1974.

Gerber, H.: Microphysics of Marine Stratocumulus Clouds with Two Drizzle Modes, J. Atmos. Sci., 53, 1649–1662, 1996.

Gerber, H., Jensen, J. B., Davis, A. B., Marshak, A., and Wiscombe, W. J.: Spectral Density of Cloud Liquid Water Content at High Frequencies, J. Atmos. Sci., 58, 497–503, 2001.

Kaufman, Y. L. and Fraser, R. S.: The effect of smoke particles on clouds and climate forcing, Science, 277, 1636–1639, 1997.

Khain, A., Pokrovsky, A., Pinsky, M., Seifert, A., and Phillips, V.: Simulation of Effects of Atmospheric Aerosols on Deep Turbulent Convective Clouds Using a Spectral Microphysics Mixed-Phase Cumulus Cloud Model. Part I: Model Description and Possible Applications, J. Atmos. Sci., 61(24), 2963–2982, 2004.

King, W. D., Dye, J. E., Strapp, J. W., Baumgardner, D., and Huffman, D.: Icing Wind Tunnel Tests on the CSIRO Liquid Water Probe, J. Atmos. Ocean. Tech., 2, 340–352, 1985.

Koren, I., Kaufman, Y. J., Remer, L. A., and Martins, J. V.: Measurement of the Effect of Amazon Smoke on Inhibition of Cloud Formation, Science, 303, 1342–1345, 2004.

Nober, F., Graf, H. F., and Rosenfeld, D.: Sensitivity of the global circulation to the suppression of precipitation by anthropogenic aerosols, Glob. Plan. Chan., 37, 57–80, 2003.

Oliveira, J. C. P. and Vali, G.: Calibration of a photoelectric cloud condensation nucleus counter, Atmos. Res., 38, 237–248, 1995.

Parikh, J.: PM2.5 Tapered Element Oscillating Microblance Procedure. State of Washington – Department of Ecology – Air Quality Program, 42 pp., 2000.

Patashnick, H. and Rupprecht, E. G.: Continuous PM-10 measurement using the tapered element oscillating microbalance, J. Air Waste Manag. Assoc., 41, 1079–1083, 1991.

Radke, L. F., Coakley Jr., J. A., and King, M. D.: Direct and Remote Sensing Observations of the Effects of Ships on Clouds, Science, 246, 1146–1149, 1989.

Reid, J. S., Hobbs, P., Rangno, A. L., and Hagg, D. A.: Relationships between cloud droplet effective radius, liquid water content, and droplet concentration for warm clouds in Brazil embedded in biomass smoke, J. Geophys. Res., 104, 6145–6153, 1999.

Rissler, J., Swietlicki, E., Zhou, J., Roberts, G., Andreae, M. O., Gatti, L. V., and Artaxo, P.: Physical properties of the submicrometer aerosol over the Amazon rain forest during the wet-to-dry season transition – comparison of modeled and measured CCN concentrations, Atmos. Chem. Phys., 4, 2119–2143, 2004, http://www.atmos-chem-phys.net/4/2119/2004/.

Rissler, J., Vestin, A., Swietlicki, E., Fisch, G., Zhou, J., Artaxo, P., and Andreae, M. O.: Size distribution and hygroscopic properties of aerosol particles from dry-season biomass burning in Amazonia, Atmos. Chem. Phys., 6, 471–491, 2006, http://www.atmos-chem-phys.net/6/471/2006/.

Roberts, G. C., Andreae, M. O., Zhou, J., and Artaxo, P.: Cloud condensation nuclei in the Amazon Basin: "Marine" conditions over a continent?, Geophys. Res. Lett., 28, 2807–2810, 2001.

Rosenfeld, D. and Gutman, G.: Retrieving microphysical properties near the tops of potential rain clouds by multispectral analysis of AVHRR data, Atmos. Res., 34, 259–283, 1994.

Rosenfeld, D. and Lensky, M. I.: Satellite Based Insights into Precipitation Formation Processes in Continental and Maritime Convective Clouds, B. Am. Meteorol. Soc., 79(11), 2457–2476, 1998.

Rosenfeld D.: TRMM Observed First Direct Evidence of Smoke from Forest Fires Inhibiting Rainfall, Geophys. Res. Lett., 26(20), 3105–3108, 1999.

Rosenfeld, D.: Suppression of Rain and Snow by Urban and Industrial Air Pollution, Science, 287, 1793–1796, 2000.

Rosenfeld, D., Lahav, R., Khain, A., and Pinsky, M.: The Role of Sea Spray in Cleansing Air Pollution over Ocean via Cloud Processes, Science, 297, 1667–1670, 2002.

Rosenfeld, D. and Woodley, W. L.: Closing the 50-year circle: From cloud seeding to space and back to climate change through precipitation physics, Chap. 6, Cloud Systems, Hurricanes, and the Tropical Rainfall Measuring Mission (TRMM), edited by: Wei-Kuo Tao and Adler, R., 234 pp., Met. Monog., 51, 59–80, AMS, 2003.

Rosenfeld, D., Fromm, M., Trentmann, J., Luderer, G., Andreae, M. O., and Servranckx, R.: The Chisholm firestorm: observed microstructure, precipitation and lightning activity of a pyro-cumulonimbus, Atmos. Chem. Phys., 7, 645–659, 2007, http://www.atmos-chem-phys.net/7/645/2007/.

Twomey, S.: Pollution and the planetary albedo, Atmos. Environ., 8, 1251–1256, 1974.

Twomey, S.: The influence of pollution on the short wave albedo of clouds, J. Atmos. Sci., 34, 1149–1152, 1977.